Supporting Information

Interface Electrostatics Dictates the Electron Transport via Bio-Electronic Junctions

Kavita Garg,[*,†] Sara Raichlin,[‡] Tatyana Bendikov,[§] Israel Pecht,[*,ǁ] Mordechai Sheves,[*,†] and David Cahen[*,‡]

[†]Department of Organic Chemistry, [‡]Department of Materials and Interfaces
[§]Department of Chemical Research Support, and [ǁ]Department of Immunology,
Weizmann Institute of Science, Rehovot 7610001, Israel
E-mail: kavitachemistry1@gmail.com; mudi.sheves@weizmann.ac.il;
david.cahen@weizmann.ac.il

Section 1. Differences in the properties of Batch (I) and Batch (II) wafers

Properties	**Batch (I)**	**Batch (II)**
Time to grow oxide in Piranha	30 s	180 s
Thickness of SiO_2 (Å)	10-11	9-11
Thickness of APTMS (Å)	6-8	5-6
Specific resistivity (mΩ*cm)	1.1-1.5	0.7-0.9
Work function of SiO_2 (UPS) (eV)	4.47	4.33
Current density for Si/SiO_2/Au Junction @ 100mV (A/cm^2)	0.6	0.03
I-V shape (Si/SiO_2/Au) (-0.5V to +0.5V)	Non-linear	Linear
Si/SiO_2/Au Junction: Ea (meV) from current T-dependence	5	20
Si/SiO_2/APTMS/OTG-bR /Au: Ea (meV) from current T-dependence	500	20
XRD of Si/SiO_2	same	same

Batch (I) and (II) *p*-Si (100) wafers were both purchased from Virginia Semiconductor Inc. with similar specific resistivity of ~1.0 mΩ cm. The wafers had a different response to controlled growth of fresh SiO_2 using piranha. On wafers from batch (I) 30s sufficed to grow oxide, whereas on batch (II) wafers it took 180s to grow oxide of the same thickness (1 nm). Since the oxides on these two types of wafers did not yield the same thickness of APTMS, all the characterizations were done with freshly grown SiO_2. XRD of both the wafers showed that both have (100) orientation. To understand the differences in the quality of oxides we did UPS measurements, which showed that batch (I) oxide has 140 meV higher work function than batch (II) oxide.

To understand the differences in the electrical properties of the oxides, I-V measurements were done using Au leaf as a top contact. The shape of the I-V curves was found to be different in that with batch (I) it was non-linear whereas with batch (II) it was linear (Fig S1 and Table S1). On Landauer modeling of these I-V curves,[1] we found that coupling (Γ) and barrier (ε) are higher for batch II wafer than batch I wafers. Γ and ε are calculated from eq.1 by fitting the I-V data.

$$I = N\frac{2e}{h}\Gamma_g^2\frac{eV}{(\varepsilon_g + \gamma eV)^2 - (\frac{eV}{2})^2}$$

Table S1. Fitting of I-V curves of Si/SiO2/Au junction to Landauer model for tunneling to extract values for energy barrier and for electrode-sample coupling.

	Batch I	**Batch II**
$\mathbf{R^2}$	0.9966	0.9992

Coupling γ (eV)	0.1291	0.3424
Barrier ε (eV)	1.3340	1.4092

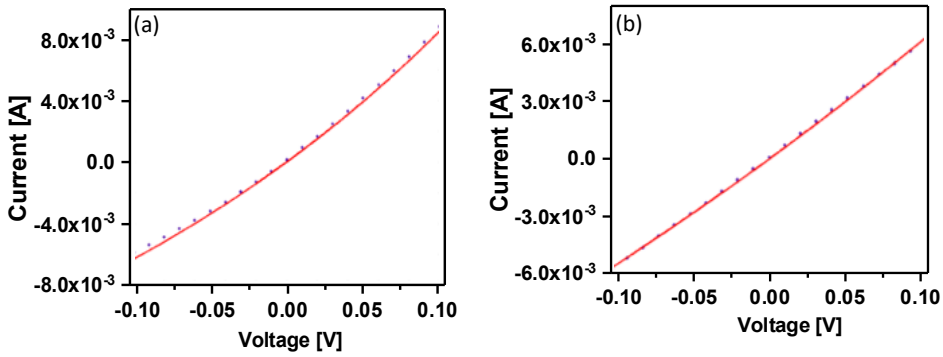

Figure S 1. Current vs. Voltage plots for Si/SiO_2/ Au (LOFO) at room temperature with different batches of wafers; red line shows Landauer fitting of the experimental data.[2] (a) Batch I (b) Batch II.

These results indicate that small variations in ultrathin oxide quality can cause significant changes in electrical properties. Moreover Batch (II) oxides showed slightly higher currents than Batch (I) oxides, which may be due slightly lower actual resistivity of Batch (II) wafers. Both the batches showed temperature independent I-V measurements from 150-300 K for Si/SiO_2/Au junctions (Fig S2), whereas for Si/SiO_2/APTMS/OTG-bR/Au junctions' batch (I) showed temperature-dependent I-V with Ea (250-400 K) of 500 meV and batch (II) showed essentially temperature-independent I-V (Ea of 20 meV could be extracted; cf. Fig S3).

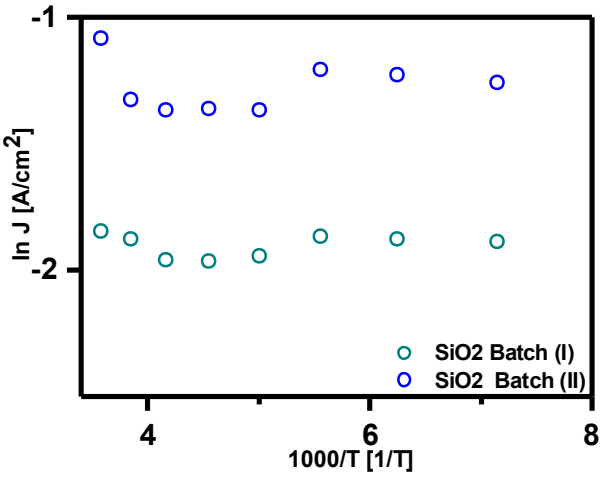

Figure S 2. Current density at 50 mV (i.e., in the linear I-V regime) plotted on logarithmic scale (ln) as a function of inverse temperature (1000/T) for Si/SiO_2/ Au(LOFO) at (150-300 K) with two different batches of Si wafers.

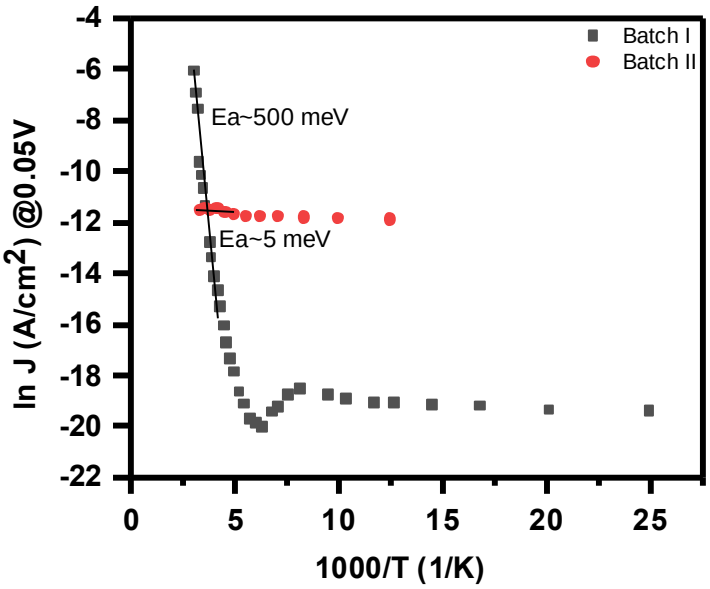

Figure S 3. Current density at 50 mV (i.e., in the linear I-V regime) plotted on logarithmic scale as a function of inverse temperature for Si/SiO_2/APTMS/OTG-bR/Au(LOFO) at (40-400 K) with two different batches of Si wafers. Ea was calculated for temperature range (250-400 K).

Section 2. Bilayers of OTG-bR

The OTG-bR layer was found to be 7-7.5 nm thick by ellipsometry. This well exceeds the largest dimension of bR, based on its known structure (~5 nm). While this large thickness is consistent with earlier reports by Ron et al.,[3] at that time this finding was explained by assuming that the vesicles retain a certain curvature upon fusion to the substrate. To check this explanation, the surface morphology of the protein was analyzed by AFM, which shows that OTG-bR forms densely-packed, ~50 nm diameter, flat circular patches on the substrate (Figure S4 and Figure 2) as we reported earlier.[4] From the AFM scans the height of these patches was found to be 9.5-10 nm. AFM scratching experiments also gave average thickness of the OTG-bR layer as ~9.5 nm (Figure 2), which is ~double the length of bR from its crystal structure.[5,6] Based on these data, we assume that, rather than having curved vesicles, the vesicles are flattened on the surface, forming protein *bilayers*. This behavior is not unusual for vesicles on a substrate, as vesicle fusion strongly depends on vesicle-surface interactions and vesicle stability in the solution.[7,8] In the case of OTG-bR it was found that OTG-bR vesicles undergo fusion during crystallization to form a 3D-hexagonal lattice, where the membranes are stacked and bR trimers are packed in an arrangement that is similar to that of bR in its native p-urple membrane environment, in a honeycomb lattice with, for OTG-bR crystals the space between the trimers filled with detergents and/or native lipids.[6] The neighboring membranes orient in opposite directions and are connected by the head- to-head and tail-to-tail interactions between the

proteins in 3D (Figure S5).[6] In the present case we propose that relatively weak electrostatic interaction of OTG-bR with the APTMS-terminated Si oxide on Si substrate and strong head-head and/or tail-tail interactions between the bR trimer layers, assisted by N_2 drying of the film, can explain the transformation of vesicles into protein bilayers.

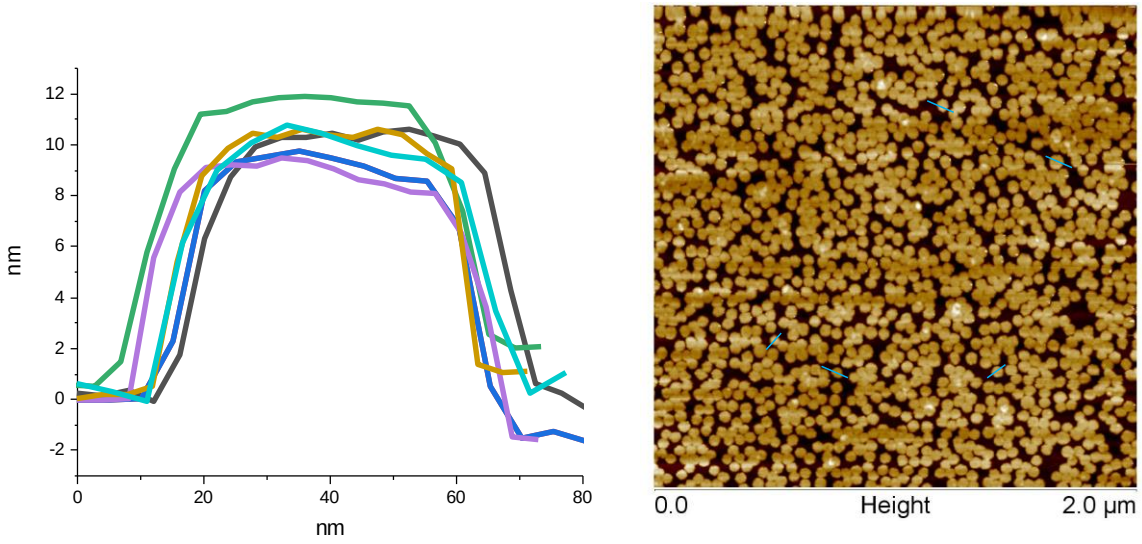

Figure S4. AFM analysis of OTG-bR to measure the height of circular patches. Line profiles were taken across isolated patches. Heights of the patches were found to be 9.5± 0.5 nm.

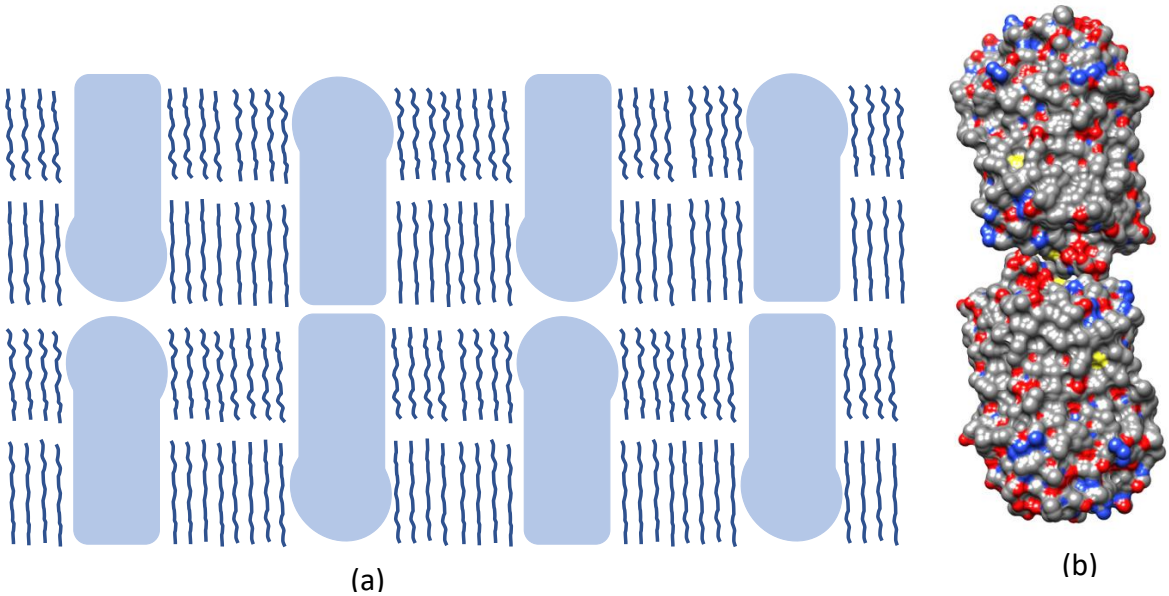

Figure S5. (a) Expected packing of bR in bilayers of bR on a surface as depicted by T. Kouyama et al. for 3D vesicular cyrstals. (b) Head-to head interactions of bR proteins in crystal structure (PDB:1fbb).

Section 3. XPS measurements

For all the APTMS-stabilized silicon oxide substrates, the Si oxide and Si wafer components were well-resolved (Fig. S7). The two broad peaks were observed at ~ 99 eV and ~103 eV, which can be deconvoluted well into five components, each component has two components Si $2p_{3/2}$ and $2p_{1/2}$. The Si $2p_{3/2}$ broad peak with the lower B.E (~99.0 eV) can be deconvoluted depending on the coordination (of O) around the Si, which can have 1, 2, and 3 oxygen atoms bound to it, making it formally Si^{+}, Si^{2+} and Si^{3+}. These peaks are assumed to be located ~ 0.95, 1.75, and 2.50 eV, respectively, from the substrate Si^{0} $2p_{3/2}$ peak, based on the assignments of Himpsel et al.[9] Note that the location of these five components can be varied slightly based on type of Silicon wafer used. The second broad peak (~ 103.0 eV) that corresponds to Si that is fully coordinated by O in SiO_2 (Si^{4+}), which is located ~ 4.0 eV from the Si substrate peak.

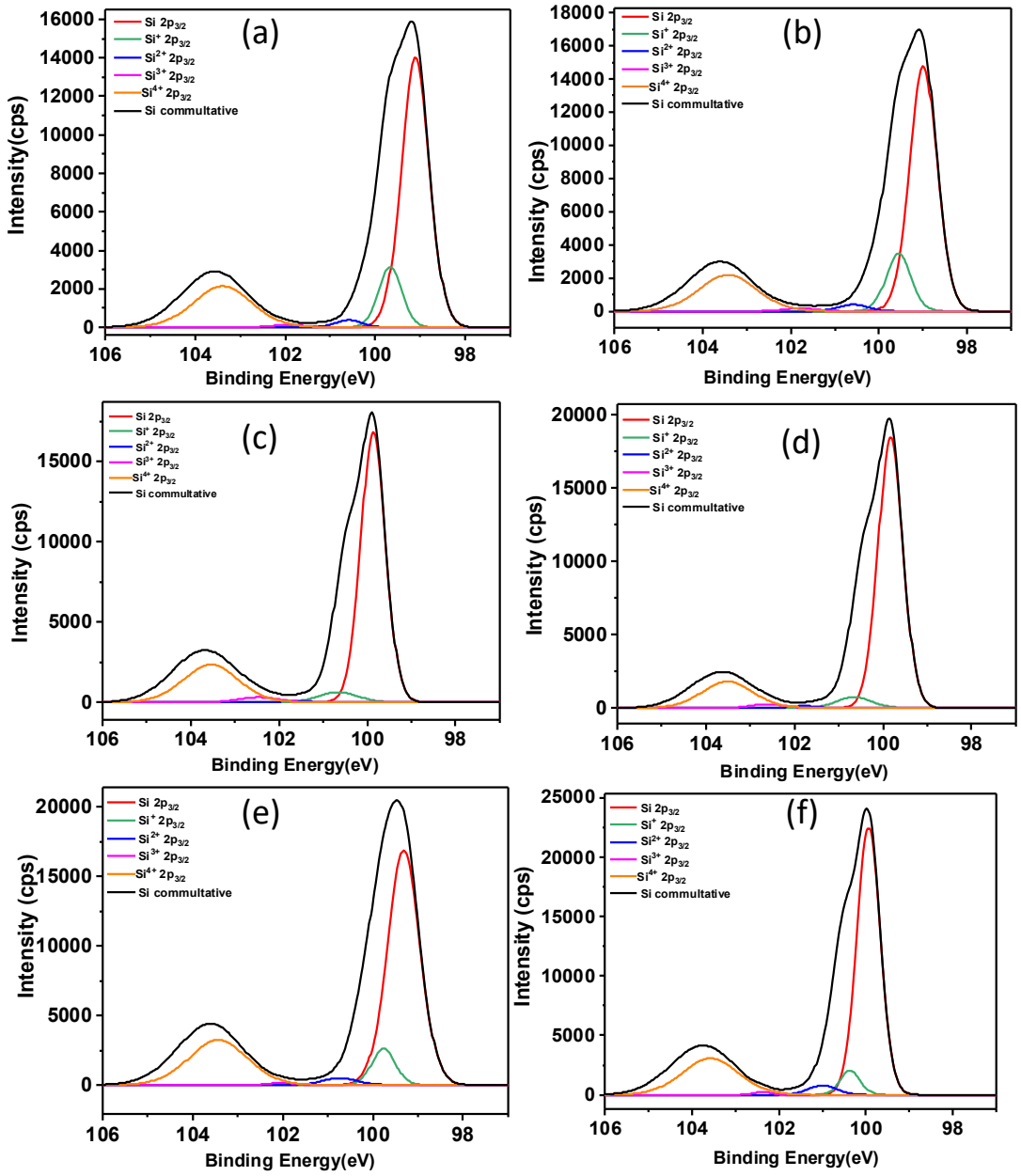

Figure S6. Deconvoluted Si 2p peak from XPS of Si/SiO_2/APTMS (a) Si (100) *p*-type HNO_3; (b) Si (100) *p*-type piranha; (c) Si (100) *n*-type HNO_3; (d) Si (100) *n*-type piranha; (e) Si (111) *n*-type HNO_3 ; (f) Si (111) *p*-type HNO_3. The Si 2p peak is deconvoluted to Si, Si^{+}, Si^{2+}, Si^{3+} and Si^{4+}, each of which has two components, Si $2p_{3/2}$ and Si$2p_{½}$. The Si $2p_{1/2}$ peaks are not shown in the figures to improve clarity.

References

(1) Walczak, K. The Role of Quantum Interference in Determining Transport Properties of Organic Molecules. *Cent. Eur. J. Chem.* **2004**, *2* (3), 524.

(2) Emberly, E.; Kirczenow, G. Electrical Conductance of Molecular Wires. *Nanotech.* **1999**, *10*, 285-283.

(3) Ron, I.; Sepunaru, L.; Ltzhakov, S.; Belenkova, T.; Friedman, N.; Pecht, I.; Sheves, M.; Cahen, D. Proteins as Electronic Materials: Electron Transport through Solid-State Protein Monolayer Junctions Proteins as Electronic Mater. *J. Am. Chem. Soc.* **2010**, *9* (4), 1–9.

(4) Jin, Y.; Honig, T.; Ron, I.; Friedman, N.; Sheves, M.; Cahen, D. Bacteriorhodopsin as an Electronic Conduction Medium for Biomolecular Electronics. *Chem. Soc. Rev.* **2008**, *37* (11), 2422–2432.

(5) Lu, Z.; Wang, J.; Xiang, X.; Li, R.; Qiao, Y.; Li, C. M. Integration of Bacteriorhodopsin with Upconversion Nanoparticles for NIR-Triggered Photoelectrical Response. *Chem. Commun.* **2015**, *51* (29), 6373–6376.

(6) Takeda, K.; Sato, H.; Hino, T.; Kono, M.; Fukuda, K.; Sakurai, I.; Okada, T.; Kouyama, T. A Novel Three-Dimensional Crystal of Bacteriorhodopsin Obtained by Successive Fusion of the Vesicular Assemblies. *J. Mol. Biol.* **1998**, *283* (2), 463–474.

(7) Reimhult, E.; Höök, F.; Kasemo, B. Vesicle Adsorption on $SiO_2$and TiO_2: Dependence on Vesicle Size. *J. Chem. Phys.* **2002**, *117* (16), 7401–7404.

(8) Keller, C. A.; Kasemo, B. Surface Specific Kinetics of Lipid Vesicle Adsorption Measured with a Quartz Crystal Microbalance. *Biophys. J.* **1998**, *75* (3), 1397–1402.

(9) Y. Yamashita; K. Namba; Y. Nakato; Y. Nishioka; H. Kobayashi. Spectroscopic Observation of Interface States of Ultrathin Silicon Oxide. *J. Appl. Phys.* **1996**, *79*, 7051.